CMOS-Integrated RF MEMS Resonators

Maxim K. Zalalutdinov, Joshua D. Cross, Jeffrey W. Baldwin, Bojan R. Ilic,
Wenzhe Zhou, *Student Member, IEEE*, Brian H. Houston, and Jeevak M. Parpia

***Abstract*—We present a design approach that enables monolithic integration of high-quality-factor (Q) radio-frequency (RF) microelectromechanical systems (MEMS) resonators with CMOS electronics. Commercially available CMOS processes that feature two polysilicon layers and field oxide isolation can be used to implement this approach. By using a nonplanar resonator geometry in conjunction with mechanical stress in polycrystalline silicon (poly) gate layers, we create rigid and robust mechanical structures with efficient electromechanical transduction. We demonstrate polysilicon domes with capacitive pickup and arch-bridge resonators with piezoresistive readout. The small footprint of our MEMS structures enables on-chip integration of large arrays of resonators for RF signal processing or sensing applications. Their large surface-to-volume ratio in combination with high rigidity (that alleviates stiction associated with wet chemistry processing) can make these resonators particularly useful for sensors that require surface functionalization. [2009-0223]**

***Index Terms*—CMOS, microelectromechanical systems (MEMS), radio frequency (RF), resonator, sensor.**

I. Introduction

THE ONGOING search for a microelectromechanical systems (MEMS) design that is compatible with commercially available CMOS processes might be compared to the search for "Cinderella's foot to fit a crystal slipper." The rigid sequence of fabrication steps implemented at a particular CMOS foundry may exclude on-chip integration for some mechanical structures and require elaborate post-CMOS processing for others [1], [2]. Hybrid integration was demonstrated as an attractive alternative [3]; however, in the case of radio-frequency (RF) MEMS resonators, it is the monolithic (on-chip) integration with CMOS electronics that is expected to open numerous possibilities for advanced signal processing [4] or sensing applications [5].

Successful monolithic integration of plate [6], beam [7]–[9], and wine glass [10] resonators in a submicrometer CMOS process (e.g., Austriamicrosystems (AMS), 0.35 μm) has been reported recently with high-Q resonators implemented in polysilicon (gate) layers and mostly utilizing in-plane motion with capacitive detection. Since the polysilicon thickness ($\approx$200 nm [8]) defines one dimension of the capacitor's plate, even with a narrow vacuum gap (interpoly oxide $\approx$40 nm was used as a sacrificial layer [10]), the value for the pickup capacitor can hardly exceed half of a femtofarad, leading to high motional resistance ($R_m \approx 3\ \mathrm{M}\Omega$) [8]. R_m is expected to be lower for the plate-type resonator reported in [6]. However, this type of structure is prone to stiction, particularly when compressive stress is present in polysilicon.

Our objective was to develop MEMS resonator designs yielding high-Q RF MEMS resonators within commercially available CMOS processes, compatible with low-resolution low-cost CMOS fab, and producing robust structures with low motional resistance. Since both RF and sensing applications are targeted, in addition to high-Q and long-term stability, the ideal structure would have a large surface-to-volume ratio and would be suitable for wet chemistry treatment, including deposition of a thin polymer layer onto the surface of the resonator in order to provide specificity toward a particular analyte of interest.

II. Design and Fabrication

In this paper, we present two micromechanical RF resonators: domes and arch bridges implemented in 1.5-μm resolution CMOS offered by ON Semiconductor (formerly AMI) through MOSIS. This process follows closely the "classic" CMOS fabrication flow described, for example, in [11]. The details (design rules, electrical and structural parameters, etc.) can be obtained from MOSIS [12]. The realization of the design is enabled by the surface curvature at the edges of the field oxide (FOX) areas. The double-tapered cross section of the FOX edge, known as the "bird's beak" (BB), is defined by the encroachment of the oxide underneath the silicon nitride mask during the thermal oxidation step [11], [13]. The length of the "beak" is comparable to the FOX thickness and is often perceived as a negative feature that limits integration density. For a MEMS designer, however, the BB presents an opportunity to create a 3-D structure within otherwise perfectly planar CMOS. A circular hole (with radius that is comparable to the BB size) opened in the middle of some "ACTIVE" polygon [14] will create a FOX "goose bump." Being conformal, the gate polysilicon layer deposited over that bump forms a shell. In the simplest mechanical structure, a single poly-layer shell can be drawn with a small opening at the apex. During post-CMOS processing, the opening in the poly layer functions as an irrigation hole for hydrofluoric acid (HF) or buffered oxide etch (BOE) to remove the underlying oxide (FOX bump), thus releasing the shell.

Manuscript received September 10, 2009; revised March 29, 2010; accepted April 10, 2010. Date of publication May 24, 2010; date of current version July 30, 2010. This work was supported in part by the Office of Naval Research and in part by the Microsystems Technology Office, Defense Advanced Research Projects Agency, under Grant HR0011-06-1-0042. Subject Editor G. K. Fedder.

M. K. Zalalutdinov was with Global Defense Technology and Systems Inc., Crofton, MD 21114 USA. He is now with the Naval Research Laboratory, Washington, DC 20375 USA (e-mail: maxim.zalalutdinov@nrl.navy.mil).

J. D. Cross, B. R. Ilic, W. Zhou, and J. M. Parpia are with Cornell University, Ithaca, NY 14853 USA (e-mail: jdc47@cornell.edu; rob@cnf.cornell.edu; wz85@cornell.edu; jeevak@ccmr.cornell.edu).

J. W. Baldwin and B. H. Houston are with the Naval Research Laboratory, Washington, DC 20375 USA (e-mail: houston@code7136.nrl.navy.mil).

Color versions of one or more of the figures in this paper are available online at http://ieeexplore.ieee.org.

Digital Object Identifier 10.1109/JMEMS.2010.2049194

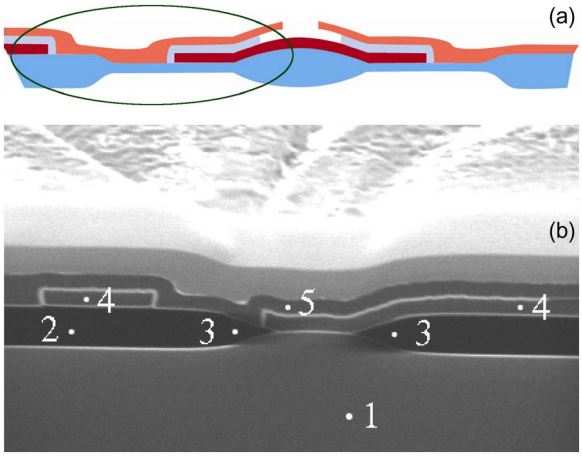

Fig. 1. (a) Schematic view of the cross section of the double-poly dome resonator. The part of the cross section encircled in (a) is shown on (b) a SEM image with Si substrate marked as (1), FOX as (2), BBs as (3), poly1 as (4), and poly2 as (5).

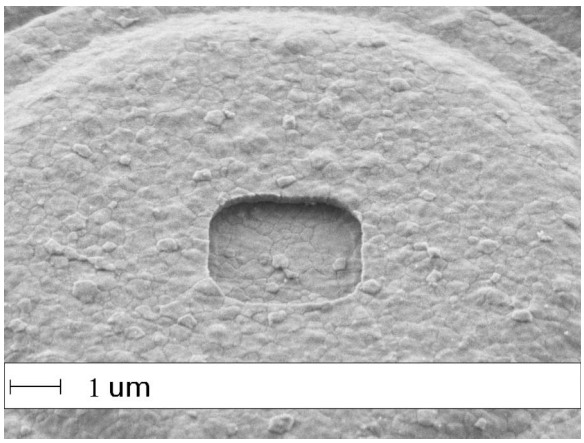

Fig. 2. Double-poly dome resonator with the vibrating shell comprising the top (poly2) layer. The interpoly oxide was used as a sacrificial layer and was removed with a wet etch, freeing the dome and revealing the bottom (poly1) layer through the etch opening.

In order to convert mechanical vibrations into an electrical signal, another layer has to be present. In our dome-type structures (cross section shown in Fig. 1), the first (bottom) polysilicon (poly1) layer does not have an irrigation hole. The poly1 "bump" stays permanently attached to the FOX (and is unaffected by the HF dip). The second (top) poly2 layer covers the poly1 layer conformally, and poly2 has an opening at the apex that is defined by the layout and therefore created when the entire poly2 layer is patterned in CMOS fabrication flow. The interpoly oxide (50-nm thermally grown oxide that normally defines a double-poly capacitor [15]) takes the role of the sacrificial layer. The wet-etch release provides a shell comprising the poly2 layer suspended over a base poly1 electrode (Fig. 2).

The dome shape of the poly2 structure is essential. An alternative structure—a flat disc with thickness h and built-in compressive stress σ clamped along the edges is expected to buckle when its radius exceeds the critical value [17]

$$R_{\text{critical}} = \sqrt{\frac{14Et^2}{12(1-\eta^2)\sigma}}. \quad (1)$$

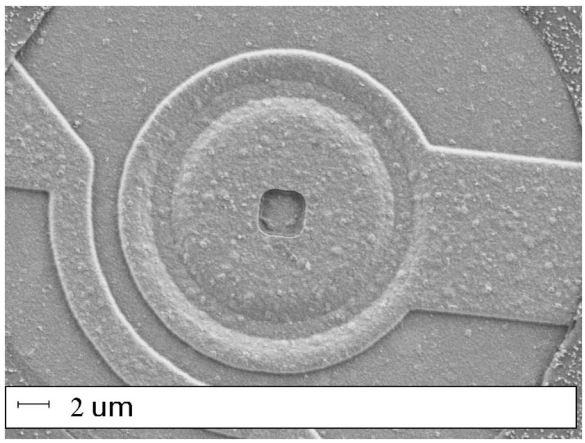

Fig. 3. "Flat-top" dome resonator with radius larger than the BB length. A thermoelastic actuator implemented as a poly1 heater is seen in the bottom left quadrant parallel to the resonator's circumference.

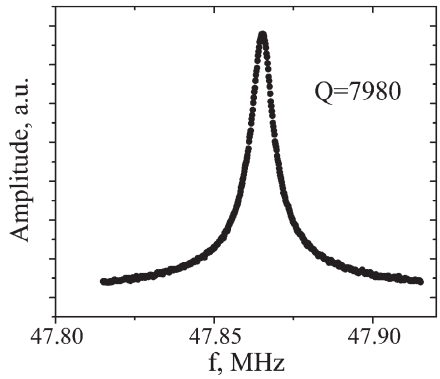

Fig. 4. Frequency response of the dome resonator acquired with thermoelastic (optical) excitation and interferometric readout [16].

For example, assuming a compressive stress $\sigma = 100$ MPa in a 320-nm-thick polysilicon film (Young's modulus $E = 170$ GPa and Poisson's ratio $\eta = 0.22$) leads to an estimate of $R_{\text{critical}} \approx 14\ \mu$m. Any slight asymmetry in the structure or surface tension during wet-etch release can lead to buckling of much smaller suspended structures. According to our observations, for a flat polysilicon film, the chances of buckling upward or snapping down into the substrate can be comparable, precluding large-scale integration [16]. In contrast to a flat disc, a compressive stress in our "precurved" (or BB-launched) dome structure will only project it upward during the release, enhancing the gap and reducing the risk of shorting the capacitor. Even domes with a radius substantially larger than the BB length do well in wet release given that the outer diameter (OD) is still within R_{critical} (domes like that display a flat top; see Fig. 3). The extra rigidity added by the dome's shape increases the resonant frequency [18] of the structure. Out of all the different resonator types we have fabricated in CMOS so far, dome resonators have shown the highest quality factor $Q = 7980$ (Fig. 4). However, two factors might limit the dome's applicability.

1) The fundamental frequency is defined by the extent of the suspended part of the dome, i.e., by the duration of the wet-etch release. In other words, all the domes on a single chip that have been co-released will have similar resonant frequencies. Some diversity can still be

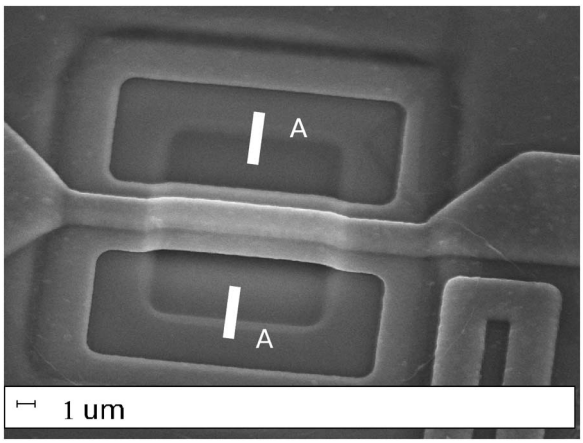

Fig. 5. "Arch-bridge" resonator. The poly1 band along the center line of the bridge was used for piezoresistive readout. A broader poly2 stripe blankets the device, providing partial protection to interpoly oxide during release. A thermoelastic actuator (poly1 meander, also covered by poly2 blanket) is shown in the right bottom corner.

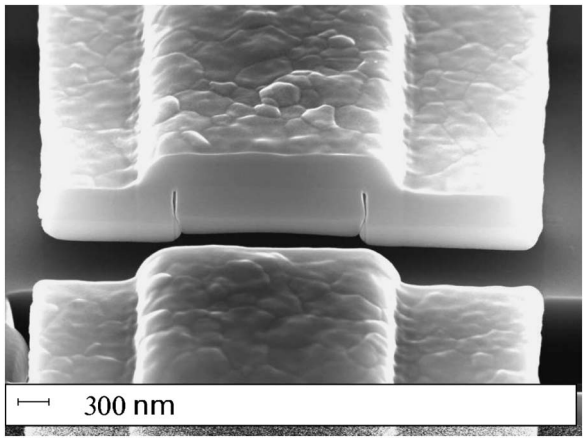

Fig. 6. Cross section of the "arch-bridge" resonator along the line shown by A-A markers in Fig. 5. The image shows the integrity of the bond between the top of the poly1 slab and the bottom of the poly2 cover.

introduced by varying, for example, the diameter of the irrigation hole at the dome's apex. However, covering a substantial frequency range by a collection of resonators on a single chip can be challenging.

2) The vulnerability associated with the narrow gap in the design. To our best knowledge, all demonstrated CMOS-integrated high- Q MEMS resonators are based on capacitive transduction and therefore are subject to this vulnerability. The high rigidity of our dome resonators and the protection of the gap provided by the suspended shell (as opposed to a fully exposed lateral gap, featured by in-plane vibrating devices [7]) can mitigate, but not eliminate, the problem.

A search for a CMOS-compatible MEMS resonator with natural frequency defined solely by layout, as opposed to the release procedure (i.e., wet etch timing) and without narrow gaps leads us to an arched bridge architecture (Fig. 5). The curvature of such a bridge is defined by the BB as well, but in contrast to the dome resonators, the sacrificial layer for the bridge is the FOX itself. The layout for the arch bridge starts with a rectangular shape drawn on the FOX layer, which produces a "pillow-shaped" SiO_2 slab. The poly1–poly2 stripe spanning across this slab adopts the out-of-plane curvature of the FOX pillow, creating an arch. As it was in the dome case, the arch can have a flat top if the width of the FOX rectangle is larger than the BB length. By dissolving the FOX, one can create a suspended structure that can be viewed as a clamped-clamped beam comprising a solid three-layer stack: poly1-interpoly oxide-poly2. The end parts of the poly stripe that extend over the FOX area form the anchoring points of the bridge. Since the interpoly oxide is located close to the center plane of the suspended beam, the out-of-plane vibrations produce a time-variable in-plane mechanical stress that is always unidirectional within each single poly layer. We utilize the piezoresistive properties of polysilicon to monitor the stress variation and thus transduce the motion of the resonator.

The integrity of the multistack bridge is crucial. Ideally, the wet etch would dissolve the sacrificial FOX layer without affecting the interpoly oxide, thus avoiding delamination of the bridge. The wide wing layout shown in Fig. 5 allows us to minimize the exposure time of the interpoly oxide to HF, without violating the design rules on the minimum spacing allowed between the poly1 and poly2 edges. By modifying the wet-etch chemistry, one can also inhibit the narrow gap etch rate (interpoly and gate oxide). Such an effect can be achieved by adding glycerol to the BOE (3:5), which leads to an increased viscosity. A cross section of the suspended part of the arch bridge released in the glycerol–BOE mixture is shown in Fig. 6. The crucial bonding between the poly1 top and poly2 cover appears to be undamaged by the release procedure. The exact mechanism of the "side-pocket" formation (≈30-nm-wide openings between the poly1 spine and poly2 sidewalls) is debatable. The electrical test shows that poly1 and poly2 are isolated after the release procedure, and these side pockets do not seem to affect the quality factor.

Similar laminated (poly–oxide–poly) vibrating structures with piezoresistive readout can also be implemented as a flat plate (double clamped bridge or U-shaped cantilever similar to that in [19]). Similar structures can be fabricated in double-poly CMOS or can be implemented in a SOI-based CMOS fabrication flow by using a single-crystal silicon (SOI) layer—gate oxide—gate polysilicon stack for the resonator. The suspended structures would have to be anchored by larger supporting pads placed on the FOX. In order to keep the undercut of the supporting pads under control, the wet etch of the flat bridges has to be timed. We expect to find arch bridges as the most tolerant, flat bridges as moderately sensitive, and dome resonators as the most affected by variations in the wet-etch time.

The dome resonators and arch bridges for our experiments were cofabricated on a single chip. The beginning of the post-CMOS processing is also common: In order to remove the silicon nitride cap layer and the interlayer dielectrics (ILDs) from the top of the resonators, we used a two-step process. First, a reactive ion etch was used to open a circular well of approximately 30 μm in diameter above the resonator. This etch (14 min, CF_4, 30 sccm, 30 mtorr, 150 W) was timed to go through SiN cap and most of the ILD, but to stop well before reaching the poly layer. For many CMOS fabs, this

first step can be included in the CMOS flow by placing a window in the "OPEN GLASS" layer designated for contact pads openings (from our experience, we know that it works for the ON Semiconductors process and it was verified for AMS as well [8]). The rest of the ILD that remains on the top of the resonator after the reactive ion etching step was removed in the second step by either an HF dip (≈20 sec) or by a longer BOE–glycerol etch (≈9 min) that leaves smaller undercuts.

The remainder of the procedure is different for domes and bridges. For the domes, the release itself starts with magnetron sputtering of a 100-nm-thick Cr film in order to protect the sidewalls of the well. Optical lithography was used then to remove the Cr film from the apex of the resonator in order to open the irrigation hole. An HF wet etch was then used to dissolve the sacrificial interpoly oxide (etch rate ≈ 1.75 μm/min) and thus release the dome. Sidewall protection during the wet etch is critical in order to avoid undercutting the ILD outside the resonator well, which otherwise would ruin the surrounding electronics (HF would dissolve the ILD approximately an order of magnitude faster than the thermally grown oxide that comprises the sacrificial layer). The release procedure is completed by stripping off the remaining Cr film.

To release the arch-bridge resonators once the ILD has been removed from the resonator's well, a new layer of photoresist with windows opened to expose the bridges was used as a mask for ≈70-min BOE–glycerol etch in order to undercut the bridges. Our preliminary data show that the timing of the wet etch has to be optimized to reduce chip-to-chip variation of the fundamental frequencies of the arch bridges. Rinsing in acetone and methanol completes the release procedure. Owing to the high rigidity of our resonators, critical point drying is not required, and multiple rinse/air-dry cycles are easily tolerated.

III. Results and Discussion

In order to evaluate the mechanical properties of the released structures, the postprocessed CMOS chips were placed in a vacuum test chamber that provides both optical and electrical accesses. For extracting the mechanical parameters of the resonators and for sorting out damaged structures, an optical setup was used. Interferometric readout is based on cw HeNe laser (633 nm), and thermoelastic excitation is provided by an independently positioned intensity-modulated diode laser beam (405 nm) [16]. The thermal relaxation time for a disc of radius $R = 5$ μm can be estimated as

$$\tau = \frac{C\rho}{K}\left(\frac{R}{\mu_1^{(0)}}\right)^2 \approx 50 \text{ ns} \tag{2}$$

where C is the heat capacity, K is the thermal conductivity, ρ is the density of silicon, and $\mu_1^{(0)}$ is the root of a Bessel function $(J_0(\mu_1^{(0)}) = 0)$ [20]. A similar expression provides an estimate for the relaxation time in a 9-μm-long bridge of $\tau \approx 30$ ns [20]. The fact that the resonant frequencies of the mechanical structures are close to the thermal cutoff provides an effective mechanism for thermoelastic drive in the 100-MHz region. Most importantly, the optical technique allows us to evaluate the ultimate performance of the mechanical structure itself. Since no electrical connection is required, the resonators can be released in the cleanest way. For example, if the entire unprotected chip is submerged into HF the electronics will be ruined, but the domes will be released without ever being exposed to photoresist or other sources of contamination (see data in Fig. 4). For the arch-bridge resonators, a similar "blanket release" procedure and optical measurements provided us with a quality factor Q in excess of 4000.

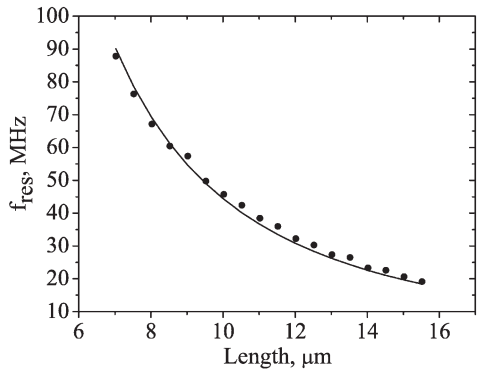

Fig. 7. Fundamental mode frequency of arch bridges (Fig. 5) as a function of bridge length (all the structures shown are co-fabricated on the same chip). Data acquired using thermoelastic (optical) excitation and interferometric readout [16]. The solid line is a fit to equation (3).

The all-optical technique was also used for the mask-released chips when the large number of the devices to be evaluated made wirebonding impractical. For example, an array of the arch-bridge resonators with increasing length was used to demonstrate the possibility of covering a substantial frequency range with a single set of on-chip devices, as shown in Fig. 7. As a guide to the eye, the plot (thin line) shows the fundamental frequency calculated for a flat doubly clamped bridge with T-shaped cross section [21]

$$f = \frac{\lambda_0^2}{2\pi L}\left(\frac{EI}{m}\right)^{1/2} \tag{3}$$

where, for the length L, we use the full span of the arch bridge (including slopes defined by BB), E is the modulus of elasticity, m is mass per unit length of the beam, and parameter $\lambda_0 = 4.73$ is defined by the boundary conditions. The moment of inertia I (about neutral axis) was calculated using the 2-μm width of the poly1 spine and the 5-μm poly2 width (wing span). The thickness of the polysilicon layer $(d = 420$ nm$)$ was used for the poly1 spine and poly2 side wings (the part of the poly2 stripe grown on FOX). Part of the poly2 layer grown on the top of the narrow ridge of poly1 spine appears to have smaller thickness, i.e., $d^* \approx 200$ nm (see Fig. 6).

For electrical measurements, two identical bridges of which only one is released (depicted by a variable resistor in Fig. 8) were placed next to each other and connected in series, creating half of a Wheatstone bridge. The poly1 stripe comprising the "spine" of the arch bridge in Fig. 5 has a resistance of 600 Ω (including leads). With such a low impedance, the central point of the bridge can be connected directly to the spectrum analyzer input (the on-chip amplifier is not required in order to test the structure).

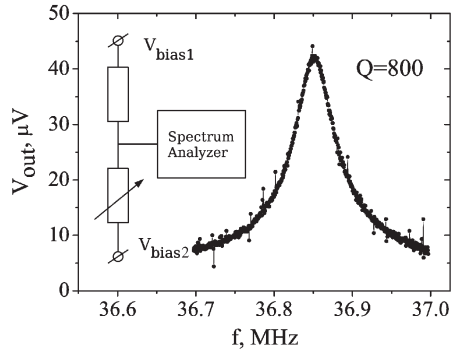

Fig. 8. Resonant response of the arch bridge acquired with piezoresistive readout. The inset shows the electrical diagram of the half-bridge and biasing used for the electrical readout.

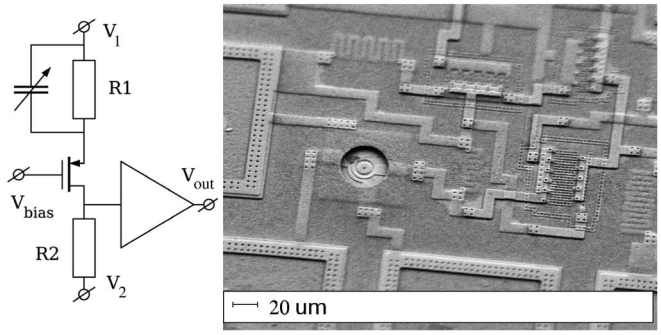

Fig. 9. Schematic diagram of the on-chip TIA (dome resonator depicted as a variable capacitor) and SEM image of the released dome integrated with TIA.

Symmetric dc biasing (± 1.5 V) and an off-chip preamplifier with five-fold gain were used to acquire the resonance curve shown in Fig. 8. The center of the resonant peak ($f_{\rm res} = 36.85$ MHz) is close to the 39-MHz fundamental frequency calculated based on a flat bridge approximation (above), assuming that the total length of the bridge is 10.5 μm (flat part, 9 μm), the width of the poly1 spine is 1.5 μm, and the poly2 width is 4.5 μm. The resonator was driven thermoelastically (optically) and showed a quality factor $Q = 800$. Piezoresistive readout with thermoelastic drive can be subject to a feedthrough due to temperature-dependent resistivity of silicon. Optical thermoelastic drive can potentially provide an additional feedthrough due to photoconductivity of silicon. Both of these mechanisms can be important, even though they are supposed to be broadband and should contribute to background as opposed to the resonant response. We are planning a detailed study of the relative contributions of these effects as well as a significant effort toward improving the efficiency of the microfabricated heater (poly1, Fig. 5). As fabricated, the heater requires an ac power in excess of 1 mW (see discussion for dome resonators hereinafter). For our next design, we are planning to use the top poly layer (electrically isolated by the interpoly oxide) for electrostatic or thermal drive. By optimizing the release procedure, we hope to bring the quality factor of the arch-bridge resonators up to the "blanket release" value $Q \approx 4000$.

In contrast to arch-bridge resonators, electrical readout for the dome resonators with capacitive transduction requires an on-chip amplifier in order to counteract the effect of parasitic capacitance associated with the connecting electrical wires. The transimpedance amplifier (TIA) with transresistance $r_m \approx 1$ kΩ was designed with a common-gate (CG) first stage [22], [23], opting for lower gain but wider bandwidth. The dome readout capacitor is connected in parallel to the source resistor of the CG stage, so that establishing the working point automatically sets the dc bias ($V_p \approx 3.6$ V) across the dome capacitor. The second stage of the amplifier (shown on the schematics as a triangle symbol) includes a common-source stage and an output buffer compatible with a 50-Ω load.

A SEM image of the released dome resonator integrated with the TIA is shown in Fig. 9. The fact that the footprint of the mechanical structure is smaller than a wirebonding pad (also true for the arch-bridge resonators) is a compelling argument for on-chip integration of RF MEMS. The resonance curve shown in Fig. 10 acquired with capacitive drive and electrical readout demonstrates a quality factor $Q = 1020$ (in vacuum, $P \approx 10^{-7}$ torr) with a center frequency of 51.36 MHz. The height of the resonance peak ($\delta S_{21}^{max} \approx \sim 10^{-3}$, background subtracted) provides us an estimate for the motional resistance $R_m^{\rm dome} \approx 740$ kΩ at $V_p = 3.6$ V. By fitting $R_m^{\rm dome}$ into the following analytical expression [3], we can calculate the effective value for the poly1–poly2 vacuum gap h as $h^* = 120$ nm (to be compared with the 55-nm initial thickness of the interpoly oxide):

$$R_m = \frac{k_s h^4}{2\pi f_{\rm res} \varepsilon^2 A^2 V_p^2 Q}. \tag{4}$$

The measured $R_m^{\rm dome}$ value for the dome resonator represents almost an order of magnitude improvement in comparison to the motional resistance $R_m^{\rm bridge} \approx 5$ MΩ recalculated for the same $V_p = 3.6$ V for the state-of-the-art CMOS-integrated double clamped bridge resonator [7]. The fact that the width of the optically detected resonance peak shown in Fig. 10 is equal to that recorded with capacitive pickup indicates that the dominating mechanism of the dissipation is unrelated to the transduction mechanism. Some resist residue that is adjacent to the dome structure visible in the SEM image is indicative of the possibility that the Q factor might be further improved by implementing a more aggressive cleaning procedure. The projected value for $R_m^{\rm dome} \approx 2.1$ kΩ based on the highest $Q = 7980$ observed in our dome resonators and $V_p = 24$ V (half of the breakdown voltage for the oxide underlying poly2 layer) might be close to the maximum achievable for the dome-type design in this particular AMI 1.5-μm CMOS process. Remarkably, this $R_m^{\rm dome}$ value for the 10-μm-OD dome resonator fabricated in the unmodified flow of the low-end CMOS process appears to be comparable to that of the 64-μm-OD wine glass resonator fabricated in a highly specialized MEMS-dedicated process: $R_m^{\rm wg} \approx 11.73$ kΩ, measured at 7 V [3] ($R_m^{\rm wg} \approx 1$ kΩ, when recalculated for $V_p = 24$ V).

The dome resonators shown in Figs. 2 and 9 were designed with the heater element implemented as a narrow (1.5-μm) poly1 arc adjacent to the dome. The heater–dome separation (2 μm, dictated by design rules) defines the efficiency of the drive and ultimately affects the insertion loss (S_{21}) of the

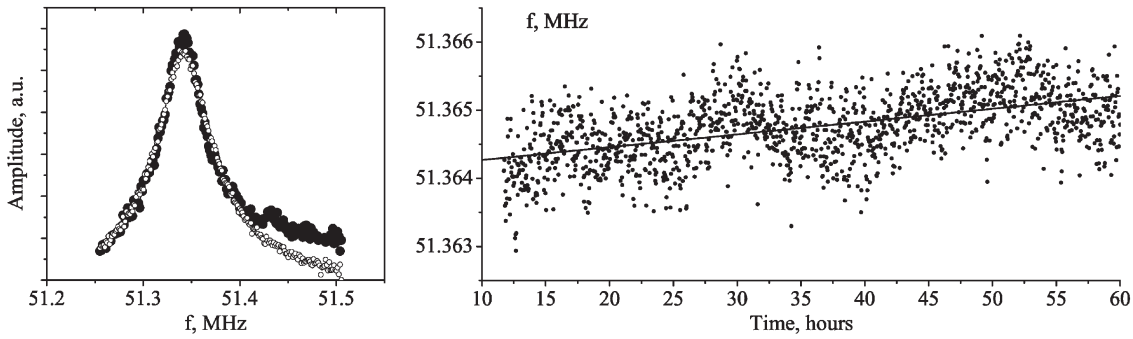

Fig. 10. (Left) Frequency response of the integrated dome resonator acquired with capacitive drive and capacitive readout (solid circles) compared to capacitive drive and optical readout (open circles). (Right) Long-term frequency stability of the integrated dome resonator (capacitive drive and readout).

overall device. We have found that such a 2-μm spacing results in an actuation ac power of $\approx$1 mW to enable a readily observable amplitude of the dome's vibration. Since thermoelastic actuation acts as an ideal mixer [24], one can reduce the required ac signal power by adding a dc offset. However, unlike with the capacitive drive, a dc bias applied to the heater actuator will dissipate additional power.

Employing a higher resolution CMOS process and moving the heater closer to the dome or placing it directly on the vibrating shell [25] will improve the drive efficiency. Our dome resonators have enough surface area for the heater to be implemented as a heavily implanted strip across the dome. In order to evaluate the ultimate efficiency of the thermoelastic drive for our dome resonators, we emulated the on-dome heater using a laser beam (diode laser, $\lambda = 405$ nm) focused on the suspended structure. Knowing the total laser power, its modulation depth, and the absorption coefficient of polysilicon at a 405-nm wavelength, we can estimate the ac power required as 50 μW, projecting $W_{\rm ac}^{\rm drive} \approx 5$ μW when dc bias is utilized.

A thermoelastic actuator with purely ohmic impedance (no reactive component) can greatly simplify impedance matching and can reduce the intermodulation [24]. However, if the figure of merit is based solely on the insertion loss, capacitive drive is a viable competitor to thermoelastic actuation. We are planning a detailed comparison of resonators with these two actuation mechanisms that would include crosstalk (thermal versus capacitive), insertion loss, and linearity considerations.

The frequency stability of MEMS RF resonators is another key parameter that can be even more important than the insertion loss for some applications. To address concerns regarding the stability of polysilicon-fabricated (as opposed to single-crystal silicon) mechanical structures, the resonance curve with capacitive drive and electrical readout (in vacuum, at room temperature) was repeatedly acquired over a 50-h period. Lorentzian fits for each peak provided the center frequency that is shown as a function of time in Fig. 10. A linear fit of the data in Fig. 10 provides us with a long-term drift of 20 Hz/h (accumulated drift $\approx$20 ppm in 50 h). From the standard deviation $\sigma \approx 420$ Hz, the short-time performance of the tested dome can be estimated: $2\sigma/f \approx 16$ ppm. The short-term stability can be compared to the half-width of the resonant peak Δf: $2\sigma \approx \Delta f/50$. The measured value for the long-term stability is close to what is expected, given a temperature coefficient of 30 ppm/°C reported for single-crystal silicon resonators [26] and temperature variations of ± 0.5 °C in our room. In a temperature-controlled environment (± 0.1 °C), long-term stability as good as $\approx$3 ppm was reported for single-crystal micromechanical resonators [26].

The demonstrated frequency stability combined with on-chip integration can enable some applications in RF communication, where microminiaturization is a key requirement (e.g., "smart dust" [27], implantable/ingestible medical devices [28], etc.). Particularly in the case of medical applications, the physical size of the device can be severely constrained, whereas the requirements for the RF performance might be relaxed given the requirements of short transmission distance and low rate of data transfer for these applications [28]. It would still take a significant improvement in motional resistance R_m before MEMS resonators similar to those described in this paper can be used as the front-end RF filters for radio receivers. However, one can envision an integrated MEMS resonator as the core of a local oscillator in a simple on-chip RF transmitter dedicated, for example, to beam out the information regarding pressure, temperature, pH, etc. In order to evaluate the performance of the dome or arch-bridge-based frequency source, we are currently working on the implementation of an integrated MEMS-based frequency generator and voltage-controlled oscillator.

Aside from the possibility of the replacement of existing off-chip components in RF devices, we anticipate that the ability to produce large arrays of low-phase-noise oscillators monolithically integrated on-chip in an affordable CMOS process will contribute toward growing interest into biologically inspired oscillator-based neural-network-type signal processing [29], [30].

For sensing applications, the short-term stability of our dome resonator σ can be projected into the added mass minimum detectable level $\delta m = 2\sigma M_R \approx 1.5$ fg in vacuum (given the mass of the dome resonator $M_R \approx 80$ pg). Based on a quality factor $Q \approx 400$ measured for a similar dome resonator in ambient conditions, we can estimate $\delta m \approx 3$ fg in air. To the best of our knowledge, this paper is the first to present monolithically CMOS-integrated MEMS resonators that can tolerate wet-chemistry-based functionalization. For example, photochemical methods [31], [32] can be employed to selectively coat the surface of a particular resonator, while others remain uncoated, thus introducing specificity for a particular analyte and allowing differential measurements in order to factor out temperature and pressure effects. Fabrication of large

arrays of integrated resonators covered with different selective polymers can be enabled with this technique. By setting the proper palette of the polymers, one can identify the components present in the vapor by measuring the frequency shift fingerprint of all the devices. This information could be fed into a principal component analysis or artificial neural network algorithm to evoke recognition of a particular analyte [33].

IV. Conclusion

We have presented a design approach that allows monolithic CMOS integration of high quality factor ($Q \approx 10^3$–10^4) RF ($f_{\rm res} \approx 10$–100 MHz) MEMS resonators. The test structures, namely, dome resonators (a thin shell implemented in top polysilicon layer) with capacitive transduction and multilayer arch-bridge resonators with piezoresistive readout, were fabricated within an unmodified flow of a standard CMOS processes (AMI, 1.5-μm minimum feature size). Our design approach can be suitable for a variety of commercially available CMOS processes that feature double polysilicon layers and FOX isolation. The concept of the multilayer bridge-type resonator design with piezoresistive transduction might potentially be extended toward SOI-based CMOS.

For the dome resonators, we provide an estimate for the motional resistance $R_m \approx 740$ kΩ at a bias voltage of 3.6 V. This represents a significant improvement over previously reported CMOS-integrated beam resonators. We demonstrate a 20-ppm long-term frequency stability (50 h) for dome resonators and short-term stability $\delta f/f \approx 16$ ppm. Although inferior to quartz crystals, CMOS-integrated MEMS resonators can find some applications in the areas where spectral purity is an affordable tradeoff for microminiaturization.

In contrast to previously presented CMOS MEMS resonators, our design either completely avoids employing narrow gaps (arch bridges) or at least has the gap protected (hidden underneath the structure—domes). Structures can be air-dried after immersion into liquids (no critical point dry required), thus enabling surface functionalization required for sensing applications. Based on the frequency stability data, we project the added mass minimum detectable level of 1.5 fg in vacuum and 3 fg in air for dome resonators.

We consider the refining of the excitation methods (thermoelastic and/or capacitive) as the next major step required to improve the performance of our devices. This would include a comparative study of the capacitive and thermal feedthrough as well as insertion loss associated with each method. Exploring temperature stability and dispersion of the resonant frequency caused by the variations in post-CMOS processing will also be necessary to define the areas of applicability for domes and bridge-type resonators. Finally, in order to expand the frequency range for dome resonators and bridges, we are planning to migrate toward higher resolution CMOS processes.

Acknowledgment

The authors would like to thank Dr. W. Lane and Dr. H. Berney at Analog Devices, Inc., for the fruitful discussions.

References

[1] G. K. Fedder, R. T. Howe, T.-J. K. Liu, and E. P. Quevy, "Technologies for cofabricating MEMS and electronics," *Proc. IEEE*, vol. 96, no. 2, pp. 306–322, Feb. 2008.

[2] W.-L. Huang, Z. Ren, Y.-W. Lin, H.-Y. Chen, J. Lahann, and C. T. C. Nguyen, "Fully monolithic CMOS nickel micromechanical resonator oscillator," in *Proc. 21st IEEE Int. Conf. MEMS*, Tucson, AZ, Jan. 13–17, 2008, pp. 10–13.

[3] Y. Lin, S. Li, Z. Ren, and C. Nguyen, "Low phase noise array-composite micromechanical wine-glass disk oscillator," in *IEDM Tech. Dig.*, Washington, DC, Dec. 5–7, 2005, pp. 287–290.

[4] C. T. C. Nguyen, "MEMS technology for timing and frequency control," *IEEE Trans. Ultrason., Ferroelectr., Freq. Control*, vol. 54, no. 2, pp. 251–270, Feb. 2007.

[5] N. Jokerst, M. Royal, S. Palit, L. Luan, S. Dhar, and T. Tyler, "Chip scale integrated microresonator sensing systems," *J. Biophotonics*, vol. 2, no. 4, pp. 212–226, Apr. 2009.

[6] A. Uranga, J. Teva, J. Verd, J. Lopez, E. Torres, J. Esteve, G. Abadal, E. Perez-Murano, and N. Barniol, "Fully CMOS integrated low voltage 100 MHz MEMS resonator," *Electron. Lett.*, vol. 41, no. 24, pp. 1327–1328, Nov. 2005.

[7] J. L. Lopez, J. Verd, A. Uranga, J. Giner, G. Murillo, F. Torres, G. Abadal, and N. Barniol, "A CMOS-MEMS RF-tunable bandpass filter based on two high-Q 22-MHz polysilicon clamped-clamped beam resonators," *IEEE Electron Device Lett.*, vol. 30, no. 7, pp. 718–720, Jul. 2009.

[8] J. L. Lopez, J. Verd, J. Teva, G. Murillo, J. Giner, F. Torres, A. Uranga, G. Abadal, and N. Barniol, "Integration of RF-MEMS resonators on submicrometric commercial CMOS technologies," *J. Micromech. Microeng.*, vol. 19, no. 1, pp. 1–10, Jan. 2009.

[9] C.-C. Lo and G. K. Fedder, "On-chip high quality factor CMOS-MEMS silicon-fin resonators," in *Proc. 14th Int. Conf. Solid-State Sens., Actuators, Microsyst., Transducers/Eurosensors XXI*, Lyon, France, Jun. 10–14, 2007, vol. 1/2, pp. 2449–2452.

[10] J. Teva, G. Abadal, A. Uranga, J. Verd, F. Torres, J. L. Lopez, J. Esteve, F. Perez-Murano, and N. Barniol, "From VHF to UHF CMOS-MEMS monolithically integrated resonators," in *Proc. 21st IEEE Int. Conf. MEMS*, Tucson, AZ, Jan. 13–17, 2008, pp. 82–85.

[11] P. E. Allen and D. R. Holberg, *CMOS Analog Circuit Design*. New York: Oxford Univ. Press, 2002, p. 18.

[12] MOSIS, Fabrication Processes. [Online]. Available: http://www.mosis.com/products/fab/vendors/

[13] A. Hastings, *The Art of Analog Layout*. Upper Saddle River, NJ: Prentice-Hall, 2001, p. 91.

[14] R. J. Baker, *CMOS Circuit Design, Layout and Simulations,* 2nd ed. Piscataway, NJ: Wiley-IEEE Press, 2005, p. 83.

[15] P. E. Allen and D. R. Holberg, *CMOS Analog Circuit Design,* 2nd ed. New York: Oxford Univ. Press, 2002, p. 44.

[16] M. Zalalutdinov, K. Aubin, C. Michael, R. Reichenbach, T. Alan, A. Zehnder, B. Houston, J. Parpia, and H. Craighead, "Shell-type micromechanical oscillator," in *Proc. Smart Sens., Actuators, MEMS,* J. C. Chiao, V. K. Varadan, and C. Cane, Eds., Maspalomas, Spain, May 19–21, 2003, vol. 5116, pp. 229–236.

[17] S. P. Timoshenko and J. M. Gere, *Theory of Elastic Stability,* 2nd ed. Singapore: McGraw-Hill, 1963, ser. Mechanical Engineering Series, p. 389.

[18] R. D. Blevins, *Formulas for Natural Frequency and Mode Shape*. Malabar, FL: Krieger, 2001, p. 331.

[19] M. Li, H. X. Tang, and M. L. Roukes, "Ultra-sensitive NEMS-based cantilevers for sensing, scanned probe and very high-frequency applications," *Nat. Nanotechnol.*, vol. 2, no. 2, pp. 114–120, Feb. 2007.

[20] A. Jeffrey, *Advanced Engineering Mathematics*. Burlington, MA: Harcourt, 2002, pp. 20, 108.

[21] R. D. Blevins, *Formulas for Natural Frequency and Mode Shape*. Malabar, FL: Krieger, 2001, pp. 20, 108.

[22] B. Baker and C. Toumazou, "Low noise CMOS common gate optical preamplifier using active feedback," *Electron. Lett.*, vol. 34, no. 23, pp. 2235–2237, Nov. 12, 1998.

[23] C. Toumazou and S. Park, "Wideband low noise CMOS transimpedance amplifier for gigaHertz operation," *Electron. Lett.*, vol. 32, no. 13, pp. 1194–1196, Jun. 20, 1996.

[24] R. Reichenbach, M. Zalalutdinov, K. Aubin, R. Rand, B. Houston, J. Parpia, and H. Craighead, "Third-order intermodulation in a micromechanical thermal mixer," *J. Microelectromech. Syst.*, vol. 14, no. 6, pp. 1244–1252, Dec. 2005.

[25] R. B. Reichenbach, M. Zalalutdinov, J. M. Parpia, and H. G. Craighead, "RF MEMS oscillator with integrated resistive

transduction," *IEEE Electron Device Lett.*, vol. 27, no. 10, pp. 805–807, Oct. 2006.
[26] B. Kim, R. Candler, M. Hopcroft, M. Agarwal, W.-T. Park, and T. Kenny, "Frequency stability of wafer-scale film encapsulated silicon based MEMS resonators," *Sens. Actuators A, Phys.*, vol. 136, no. 1, pp. 125–131, May 1, 2007.
[27] J. Kahn, R. Katz, and K. Pister, "Emerging challenges: Mobile networking for "smart dust"," *J. Commun. Netw.*, vol. 2, no. 3, pp. 188–196, Sep. 2000.
[28] Y. Jui, D. Sadowski, K. Kaler, and M. Mintchev, "The ESO-Pill: A non-invasive MEMS capsule for bolus transit monitoring in the esophagus," in *Proc. 11th IEEE ICECS*, Tel Aviv, Israel, Dec. 13–15, 2004, pp. 427–430.
[29] F. Hoppensteadt and E. Izhikevich, "Synchronization of MEMS resonators and mechanical neurocomputing," *IEEE Trans. Circuits Syst. I, Fundam. Theory Appl.*, vol. 48, no. 2, pp. 133–138, Feb. 2001.
[30] F. Corinto, M. Bonnin, and M. Gilli, "Weakly connected oscillatory network models for associative and dynamic memories," *Int. J. Bifurcation Chaos*, vol. 17, no. 12, pp. 4365–4379, Dec. 2007.
[31] T. Strother, W. Cai, X. Zhao, R. Hamers, and L. Smith, "Synthesis and characterization of DNA-modified silicon (111) surfaces," *J. Amer. Chem. Soc.*, vol. 122, no. 6, pp. 1205–1209, Feb. 16, 2000.
[32] J. Baldwin, M. Zalalutdinov, B. Pate, M. Martin, and B. Houston, "Optically defined chemical functionalization of silicon nanomechanical resonators for mass sensing," in *Proc. 8th IEEE Conf. Nanotechnol., NANO*, Aug. 2008, pp. 139–142.
[33] V. S. Kodogiannis, J. N. Lygouras, A. Tarczynski, and H. S. Chowdrey, "Artificial odor discrimination system using electronic nose and neural networks for the identification of urinary tract infection," *IEEE Trans. Inf. Technol. Biomed.*, vol. 12, no. 6, pp. 707–713, Nov. 2008.

Maxim K. Zalalutdinov received the M.S. and Ph.D. degrees from Moscow State University, Moscow, Russia, in 1986 and 1989, respectively.

Since 2004, he has been with the Global Strategies Group Inc., Crofton, MD, and the Acoustics Division, Naval Research Laboratory, Washington, DC, focusing on nonlinear dynamic effects in RF nanoelectromechanical systems (NEMS) and collective behavior of large arrays of coupled NEMS resonators. His research interests include new materials and fabrication techniques for nanomechanical devices, monolithically integrated NEMS-CMOS systems, and their applications for sensing and RF signal processing.

Joshua D. Cross received the B.A. degree in physics from Lawrence University, Appleton, WI, and the Ph.D. from the Applied Physics Department, Cornell University, Ithaca, NY, with expertise in micro- and nanofabricated fluidic devices for biological applications.

After receiving the Ph.D. degree, he shifted into microelectromechanical systems (MEMS) and nanoelectromechanical systems research with a focus on integrating MEMS devices with CMOS fabrication processes and using MEMS as biological and chemical sensors. He has presented numerous contributed and invited talks at scientific conferences and before government review panels. He is the founder and CEO of Veratag, a company that is commercializing MEMS technology related to radio-frequency identification security applications. While at Cornell University, he was a founding member of a recurring event at the Johnson Graduate School of Management known as Start-up Cornell which brings preseed stage companies together with venture capital and private equity groups for critical and educational dialogue on the process of starting companies and giving presentations.

Jeffrey W. Baldwin received the B.S. degree in chemistry from Erskine College, Due West, SC, in 1996, and the Ph.D. degree in physical chemistry from the University of Alabama, Tuscaloosa, in 2002. His doctoral research was in the field of nanoscience (molecular electronics) which included surface science (X-ray photoelectron spectroscopy, scanning tunneling microscopy, Fourier transform infrared spectroscopy, atomic force microscopy) and nanofabrication techniques.

Since 2003, he has been a Research Chemist at the Naval Research Laboratory (NRL), Washington, DC, in Code 7136, primarily studying silicon and diamond nanomechanical systems. His research interests include the design, fabrication, and characterization of novel nanoelectromechanical systems (NEMS) using graphene, diamond, and silicon films for chemical and biological agent sensing and RF signal processing.

Dr. Baldwin was awarded an NRC postdoctoral fellowship to study carbon nanostructures at NRL in 2002.

Bojan R. Ilic received the B.S. degree in engineering physics and the M.S. degree in electrical engineering from the University of Illinois, Chicago, in 1996 and 1998, respectively, and the M.S. and Ph.D. degrees in applied physics from Cornell University, Ithaca, NY, in 2002 and 2006, respectively.

Since 2002, he has been a Research Staff Member and a User Program Manager at the Cornell Nanoscale Facility, Cornell University. He has authored or coauthored over 80 journal publications in the fields of optics, quantum electronics, scanning probes, electrochemical and biological sensors, micro- and nanoelectromechanical systems, nanofluidics, flux pinning in thin-film superconductors, nanomagnetics, and measurement of the quantum fluctuations of the zero-point electromagnetic field. His research interests are in the development of nanofabrication technologies for building fully integrated molecular scale devices, use of micro- and nanomechanical resonant sensors for novel chemical and biological detection schemes, nanofluidics, atomic force probes, and nanomagnetics.

Wenzhe (Wilson) Zhou (S'08) was born in Shanghai, China. He received the B.S. degree in microelectronics from Fudan University, Shanghai, China, in 2008, and the M.Eng. degree in electrical and computer engineering from Cornell University, Ithaca, NY, in 2009, where he is currently working toward the Ph.D. degree in the School of Electrical and Computer Engineering.

His research interests include design, modeling, and fabrication of RF microelectromechanical systems (MEMS) resonators, ultrasensitive MEMS structures, and CMOS-MEMS integration.

Brian H. Houston received the B.S., M.S., and Ph.D. degrees in physics from the American University, Washington, DC, in 1980, 1985, and 1989, respectively. His graduate work concerned the polarization dependence of multiphoton ionization of Nobel gases from metastable energy levels.

Since 1980, he has been with the Naval Research Laboratory (NRL), Washington, DC, where he is currently the Head of the Physical Acoustics Branch, Acoustics Division, and started the Experimental Techniques Section (Code 7136). He has developed a broad research program covering a range of science and engineering disciplines in physical acoustics. His personal areas of research include atomic and solid-state physics, micro- and nanomechanical devices, optics, and structural acoustics.

Dr. Houston is a Fellow of the Acoustical Society of America. He received the American University Ross Gunn Award for Outstanding Experimental Research, the NRL Alan Berman Research Publication Award (five times), the NDIA Special Achievement Bronze Medal, and the Navy Meritorious Civilian Service Award.

Jeevak M. Parpia received the B.S. degree in physics from Illinois Institute of Technology, Chicago, in 1973, and the M.S. and Ph.D. degrees in experimental low-temperature physics from Cornell University, Ithaca, NY, in 1977 and 1979, respectively.

In 1979, he became an Assistant Professor at Texas A&M, College Station, and was promoted with tenure in 1984. In 1986, he became an Associate Professor in the Physics Department, Cornell University, where he has been a Professor since 1992. From 2000 to 2001, he was a Visiting Fellow in the Department of Physics, Royal Holloway College, University of London, London, U.K. His current research involves studies of highly confined 3He, gases, and the role of stress on the quality factor in micromechanical resonators at low temperatures. Sensing with microelectromechanical systems is also a current research area, as is the mechanics of graphene.

Dr. Parpia was elected a Fellow of the American Physical Society in 2005. He was the recipient of an Alfred P. Sloan Fellowship in 1982 and a Guggenheim Fellowship in 1994.